PHYSICAL REVIEW E **95**, 010202(R) (2017)

# Nonvariational mechanism of front propagation: Theory and experiments

A. J. Alvarez-Socorro,[1] M. G. Clerc,[1] G. González-Cortés,[1] and M. Wilson[1,2]
[1]*Departamento de Física, FCFM, Universidad de Chile, Casilla 487-3, Santiago, Chile*
[2]*CONACYT–CICESE, Carretera Ensenada-Tijuana 3918, Zona Playitas, CP 22860, Ensenada, México*
(Received 13 June 2016; revised manuscript received 14 December 2016; published 17 January 2017)

Multistable systems exhibit a rich front dynamics between equilibria. In one-dimensional scalar gradient systems, the spread of the fronts is proportional to the energy difference between equilibria. Fronts spreading proportionally to the energetic difference between equilibria is a characteristic of one-dimensional scalar gradient systems. Based on a simple nonvariational bistable model, we show analytically and numerically that the direction and speed of front propagation is led by nonvariational dynamics. We provide experimental evidence of nonvariational front propagation between different molecular orientations in a quasi-one-dimensional liquid-crystal light valve subjected to optical feedback. Free diffraction length allows us to control the variational or nonvariational nature of this system. Numerical simulations of the phenomenological model have quite good agreement with experimental observations.

DOI: 10.1103/PhysRevE.95.010202

The coexistence between different equilibria is a characteristic property of nonequilibrium systems [1–3]. Inhomogeneous initial conditions caused by, e.g., inherent fluctuations of macroscopic systems, generate spatial domains which are separated by domain walls. These interfaces are known as front interfaces, domain walls, or wave fronts [3,4]. Interfaces between these metastable states appear in the form of propagating fronts and give rise to rich spatiotemporal dynamics [5]. Front dynamics has been observed in several contexts, such as walls separating magnetic domains, liquid-crystal phases, fluidized granular states, chemical reactions, and solidification and combustion processes, to mention a few. Indeed, front solutions are robust phenomena ranging from chemistry and biology to physics. Moreover, these propagative fronts can be regarded as particle-type solutions, i.e., they can be characterized by a set of continuous parameters such as position, core width, and so forth. Front propagation depends on the nature of the states that are being connected. For example, in the case of a front connecting a stable and an unstable state, its speed is not unique but is determined by the initial conditions [6]. This scenario changes for a front connecting two stable uniform states. For variational or gradient systems, the most stable state invades the other one, in order to minimize its nonequilibrium energy or Lyapunov functional [7]. Likewise, there is only one point in the parameter space for which the front is motionless, the Maxwell's point.

Due to a time-scale separation of the microscopic variables, the dynamics of macroscopic systems is described by a small number of variables (coarse-graining process), which generally satisfy nonvariational or nongradient equations [2–4]. In this framework, walls connecting two equivalent vectorial fields through spontaneous symmetry breaking can spread according to a given chirality of the vector field [8]. This mechanism, the nonvariational Ising-Bloch transition, is well known [9]. A deeper understanding of front propagation in macroscopic systems out of equilibrium will open the possibilities for applications in nonequilibrium crystal growth, operation of nonequilibrium magnetic and optical memories, control of nonequilibrium chemical reactions, to mention a few.

The aim of this Rapid Communication is to show that front solutions in scalar field models generically propagate based on two mechanisms: (i) the energy difference between states, and (ii) nonvariational effects. Considering a simple nonvariational bistable model, we show analytically and numerically that front propagation is led by nonvariational dynamics. A quasi-one-dimensional liquid-crystal light valve (LCLV) experiment with optical feedback allows us to evidence nonvariational front propagation between different molecular orientations. Free diffraction lengths allow us to control the variational or nonvariational nature of this optical system. A phenomenological model for small free diffraction lengths is derived. Numerical simulations of this model have quite good agreement with experimental observations.

*Simple bistable model.* Let us consider a bistable model

$$\begin{aligned}\partial_t u &= \eta + \mu u - u^3 + \partial_{xx} u + \epsilon[c(\partial_x u)^2 + bu\partial_{xx} u] \\ &= -\frac{\delta F}{\delta u} + \epsilon F_{NV},\end{aligned} \tag{1}$$

where the scalar field $u(x,t)$ is an order parameter that accounts for an imperfect pitchfork bifurcation [4], $\mu$ is a bifurcation parameter, $\eta$ stands for the asymmetry between the equilibria, $\epsilon$ is an small parameter, $\epsilon \ll 1$, that controls the nonvariational force $F_{NM} \equiv c(\partial_x u)^2 + bu\partial_{xx} u$, $\{c,b\}$ account for, respectively, nonlinear convective and diffusive terms, and the functional

$$F \equiv \int dx \left[ V(u) + \frac{(\partial_x u)^2}{2} \right], \tag{2}$$

where $V(u) \equiv -\eta u - \mu u^2/2 + u^4/4$ is a potential. Notice the above model is invariant under spatial reflection symmetry ($x \to -x$). Moreover, model (1) is variational when $b = 2c$.

For $\epsilon = 0$, the above model (1) becomes a variational one. This model has two stable equilibria for $\eta$ small and positive $\mu$, $u = \pm\sqrt{\mu} + O(\eta)$, represented by $\{\mathcal{A},\mathcal{B}\}$. Figure 1 depicts the potential $V(u)$ for different values of $\eta$. A nontrivial solution of this variational model is front waves, $u_F(x - vt) \approx \pm\sqrt{\mu}\tanh[\sqrt{\mu/2}(x - vt)] + O(\eta)$, that connect these two equilibria [7]. The middle and lower panels of Fig. 1 show the profiles of the front solutions and their respective spatiotemporal evolutions. Notice that fronts propagate at a constant speed. The location and the region of the space where

 

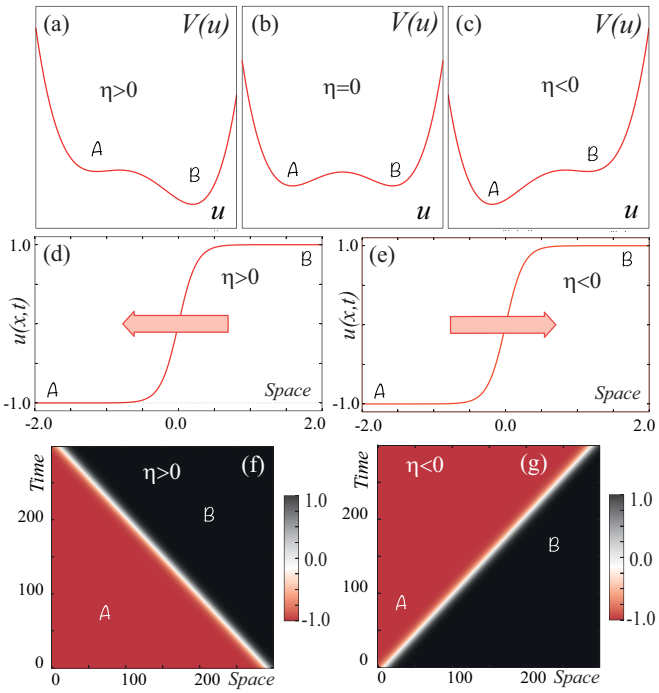


FIG. 1. Front propagation in the bistable variational model Eq. (1) with $\epsilon = 0$. The upper panels represent the potential $V(u)$ for different values of $\eta$, (a) $\eta = 0.2$, (b) $\eta = 0$, and (c) $\eta = -0.2$, with $\mu = 1.0$. The middle and lower panels illustrate the front profiles and their respective spatiotemporal evolutions for (d), (f) $\mu = 1.0$, $\eta = 0.3$, and (e), (g) $\eta = -0.3$.

the front has a greater variation is known as the front position and core, respectively. In the pioneering work of Pomeau [7], it was shown that the front speed $v$ is ($\eta \ll 1$)

$$v = v_V \equiv \frac{V(\mathcal{A}) - V(\mathcal{B})}{\int_{-\infty}^{\infty} (\partial_x u_F)^2 dx} \approx \frac{3\sqrt{2}}{2\mu}\eta. \tag{3}$$

Hence, the front speed is proportional to the energy difference between the equilibria and the front core shape (denominator). Indeed, the most energetically favorable state invades the least favorable one (cf. Fig. 1). Likewise, when both states have the same energy, $\eta = 0$, the front is motionless, which corresponds to Maxwell's point. Therefore, for variational systems the mechanism of front propagation is the energy difference between the connected equilibria.

In the case where nonvariational terms are considered, $\epsilon \neq 0$, the above scenario changes drastically. To figure out these changes, we consider model Eq. (1) at Maxwell's point and the nonvariational terms as perturbative, $\epsilon \ll 1$. Then, in this limit we can use the following ansatz for the front solution, $u(x,t) = u_F(x - vt) + w(x - vt, v)$, where $w$ is a small adjustment function, which is of order of $\epsilon$. Using this ansatz in Eq. (1), linearizing in $w$, and imposing solvability conditions, we get

$$v_{NV} \equiv \epsilon \frac{c\int_{-\infty}^{+\infty} (\partial_x u_F)^3 dx + b\int_{-\infty}^{+\infty} u_F \partial_x u_F \partial_{xx} u_F dx}{\int_{-\infty}^{+\infty} (\partial_x u_F)^2 dx}. \tag{4}$$

Then, the front speed is proportional to the nonvariational terms. Notice that a similar method to obtain the speed of the propagative front was used to characterize the Ising-Bloch transition [9].

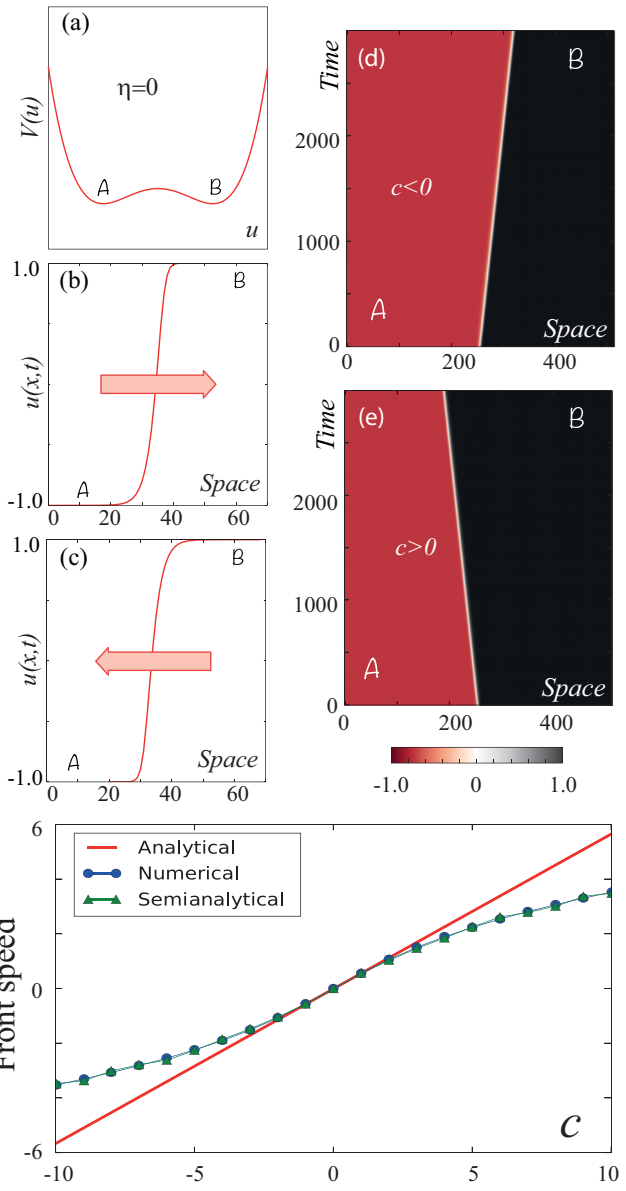


FIG. 2. Nonvariational front propagation model Eq. (1) at Maxwell's point ($\eta = 0, \epsilon = 1$, and $\mu = 1$). (a) Potential $V(u)$. Front profiles at a given instant for (b) positive $c = 3$, (c) negative $c = -3$, and $b = 0$. (d) and (e) represent the spatiotemporal evolutions of front solutions with positive and negative parameters $c$ respectively and $b = 0$. (f) Dimensionless front speed as a function of parameter $c$. Points account for the numerical front speed obtained from Eq. (5) with $b = 0$, $\eta = 0$, and $\epsilon = 1$, the solid straight line is obtained from the analytical formula $v_{NV} \approx (2c - b)\epsilon\mu\sqrt{2}/5$, and the curve is obtained using formula (4) with a numerical front profile $u_F$.

From the above formula, we can conclude that the mechanism generating the spread of this front is only the front shape. Namely, the front core shape [$\partial_x u_F \sim O(1)$] determines the propagation speed and not the energy difference between equilibria. The above expression can be approximated by $v_{NV} \approx (2c - b)\epsilon\mu\sqrt{2}/5$. Figure 2 illustrates the nonvariational front propagation observed from the model (1) for

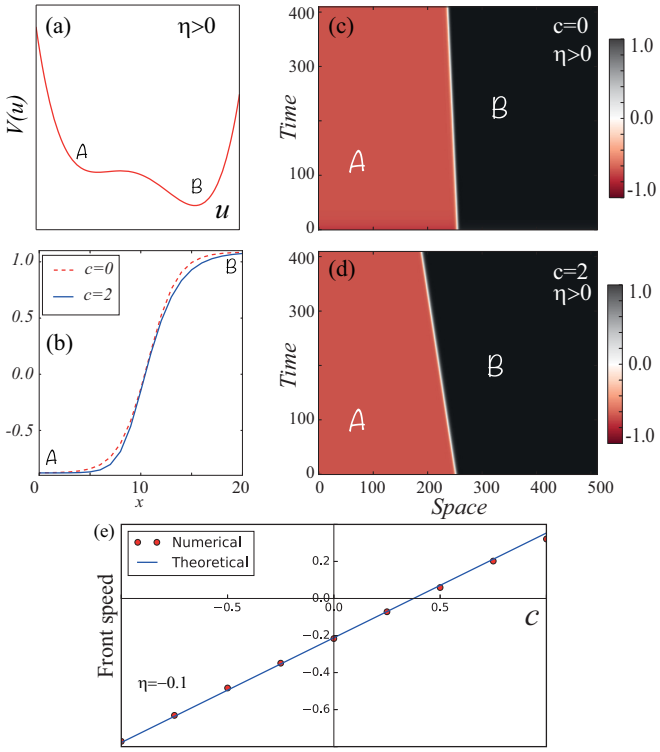


FIG. 3. Front propagation model Eq. (1) with $\eta = 0.3$ and $\mu = 1$. (a) Potential $V(u)$. (b) Front profiles for zero (dashed line) and positive (solid line) $c$ and $b = 0$. (c) and (d) represent the spatiotemporal evolutions of the front solution with zero and positive parameter $c$. (e) Dimensionless front speed as a function of parameter $c$. Points account for the numerical front speed and continuous curve $v = v_V + v_{NV}$.

different values of parameter $c$. For small $c$, the system exhibits quite good agreement with the above approximation. For large $c$, we can use formula (4) with $u_F$ obtained numerically. This semianalytical approach has quite fair agreement (cf. Fig. 2). Notice that nonlinear convection and diffusion are opposite effects for front speed. The front becomes motionless when the system is variational ($b = 2c$).

When considering the general case of asymmetry between equilibria ($\eta \neq 0$) and the presence of nonvariational terms, the front speed is determined by the two mechanisms discussed above, i.e., the front speed is $v = v_V + v_{NV}$. Figure 3 depicts the front propagation in the generic case. A comparison between numerical simulations and theoretical results shows quite good agreement (cf. Fig. 3). Note that there is always a point in the parameter space where the front is motionless ($v_V = -v_{NV}$), but which does not correspond to equal energy between states.

*Liquid-crystal light valve with optical feedback.* A simple physical system that exhibits nonvariational behaviors and multistability is a LCLV with optical feedback [10–13]. This setup contains a LCLV inserted in an optical feedback loop (see Fig. 4). The LCLV is composed of a nematic liquid-crystal film sandwiched in between a glass and a photoconductive plate over which a dielectric mirror is deposited (see Ref. [11] and references therein). The feedback loop is closed by an optical fiber bundle (FB) and is designed in such a way that diffraction and polarization interferences are simultaneously present. The optical free propagation length is given by $L$.

The liquid-crystal film under consideration is planarly aligned (nematic director $\vec{n}$ parallel to the walls), with a thickness $d = 15\ \mu$m. The liquid crystal filling the LCLV is a nematic LC-654, produced by NIOPIK. It is a mixture of cyanobiphenyls, with a positive dielectric anisotropy $\Delta\varepsilon = \varepsilon_\parallel - \varepsilon_\perp = 10.7$ and a large optical birefringence $\Delta n = n_\parallel - n_\perp = 0.2$, where $\varepsilon_\parallel$ and $\varepsilon_\perp$ are the dielectric permittivities $\parallel$ and $\perp$ to $\vec{n}$, respectively, and $n_\parallel$ and are $n_\perp$ are the extraordinary ($\parallel$ to $\vec{n}$) and ordinary ($\perp$ to $\vec{n}$) refractive indices [14]. Transparent electrodes over the glass plates allow for the application of an electrical voltage $V_0$ across the nematic layer. The photoconductor behaves as a variable resistance, which decreases for increasing illumination. The light which has passed through the liquid-crystal layer and has been reflected by the dielectric mirror experiences a phase shift which depends on the liquid-crystal molecular orientation and, at its turn, modulates the effective voltage that is locally applied to the liquid-crystal sample. Over a critical voltage, the molecules tend to orient along the direction of the applied electric field,

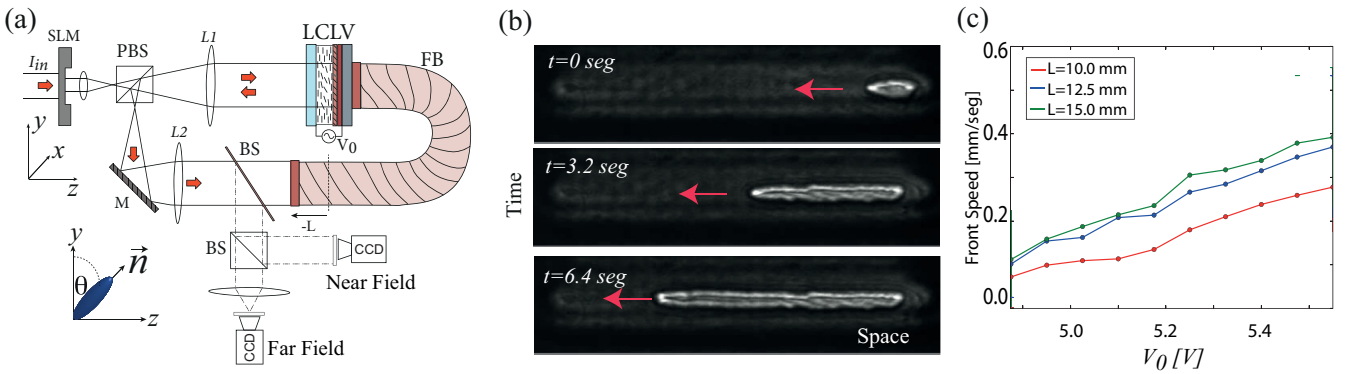


FIG. 4. Nonvariational front propagation in a LCLV with optical feedback. (a) Schematic representation of the experimental setup. $\{L1, L2\}$ stands for two lenses with a focal distance $f = 25$ cm, M is a mirror, FB is an optical fiber bundle, PBS is a polarizing beam splitter cube, BS represents a beam splitter, and SLM is a spatial light modulator driven by a computer. $V_0$ external voltage applied across the LCLV. (b) Temporal sequence of snapshots of front propagation from top to bottom. (c) Front speeds as a function of voltage $V_0$ for different free propagation lengths $L$.

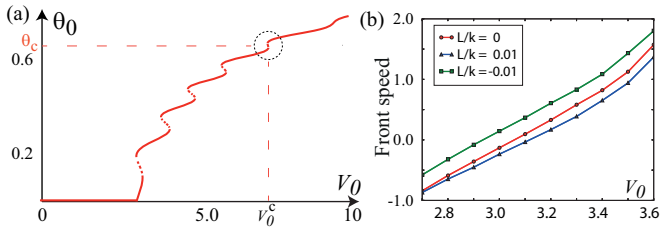


FIG. 5. Front propagation of the numerical simulation of the phenomenological model of LCLV with optical feedback Eq. (5). (a) Bifurcation diagram of molecular average orientations $\theta_0$ as a function of voltage $V_0$. $V_0^c$ accounts for a critical value of voltage for which the system exhibits nascent bistability at $\theta_0 = \theta_c$. (b) Front speeds as functions of voltage $V_0$ for different free propagation lengths.

which changes local and dynamically following the spatial distribution of illumination present in the photoconductor wall of the cell. When liquid-crystal molecules reorient, due to their birefringent nature, they induce a refractive index change. Thus, the LCLV acts as a manageable Kerr medium, causing a phase variation $\phi = \beta \cos^2\theta \equiv 2kd\Delta n \cos^2\theta$ in the reflected beam proportional to the intensity of the incoming beam $I_w$ on the photoconductive side, where $\theta$ is the longitudinal average of the molecular reorientation. Here, $k = 2\pi/\lambda$ is the optical wave number. The LCLV is illuminated by an expanded He-Ne laser beam, $\lambda = 633$ nm, with a 1 cm transverse diameter and power $I_{in} = 6.5$ mW/cm$^2$, linearly polarized along the vertical $y$ axis. A spatial light modulator (SLM, controlled through an external computer) was placed in the input beam in order to carry out one-dimensional experiments. The system dynamics is controlled by adjusting the external voltage $V_0$ and free propagation length $L$.

*Theoretical description of the LCLV.* The light intensity $I_w$ reaching the photoconductor is given by $I_w(\theta,L) = I_{in}|e^{-i\frac{L}{2k}\partial_{xx}}(1+e^{-i\beta\cos^2\theta})|^2/2$ [11], where $x$ is the transverse direction of the liquid-crystal layer. As long as $I_{in}$ is sufficiently small ($I_{in} \sim 1$ mW/cm$^2$), the effective voltage $V_{\rm eff}$ applied to the liquid-crystal layer can be expressed as $V_{\rm eff} = \Gamma V_0 + \alpha I_w$, where $0 < \Gamma < 1$ is a transfer factor that depends on the electrical impedances of the photoconductor, dielectric mirror, and the liquid crystal, while $\alpha$ is a phenomenological dimensional parameter that describes the linear response of the photoconductor [11].

The dynamics of the average director tilt $\theta(x,t)$ is described by a nonlocal relaxation equation of the form [10]

$$\tau\partial_t\theta = l^2\partial_{xx}\theta - \theta + \frac{\pi}{2}\left(1 - \sqrt{\frac{\Gamma V_{\rm FT}}{\Gamma V_0 + \alpha I_w(\theta,L)}}\right), \quad (5)$$

with $V_{\rm FT} \approx 3.2$ V$_{\rm rms}$ the threshold for the Fréedericksz transition, $\tau = 30$ ms the liquid-crystal relaxation time, and $l = 30$ $\mu$m the electric coherence length.

Let us consider the zero free propagation length, $L = 0$, $I_w(\theta, L=0) = I_{in}\{1+\cos(\beta\cos^2\theta)\}/2$. In this limit, Eq. (5) is a gradient model. To derive a simple description of the above model, we study its dynamics around the emergence of bistability, i.e., when the system becomes multivalued or exhibits nascent bistability [15]. Figure 5(a) depicts nascent bistability. We express the expression for equilibria $\theta(x,t) = \theta_0$ as follows, $V_0(\theta_0) = V_{\rm FT}/\Gamma(1 - 2\pi^{-1}\theta_0)^2 - \alpha I_{in}[1+\cos(\beta\cos^2\theta_0)]/2\Gamma$, and from this relation we determine the values of the parameters for the emergence of bistability. Indeed, in the parameter space, the above expression generates a folded surface from which one can geometrically infer the points of nascent bistability [cf. Fig. 5(a)]. In fact, $\theta_0$ becomes multivalued when the function $V_0(\theta_0, I_{in})$ has a saddle point at $\theta_0 = \theta_c$. Around the saddle point $V_0(\theta_c)$ creates two new extreme points that determine the width of the bistability region. To find the saddle points of $V_0(\theta_c, I_{in})$, we have to impose the conditions $dV_0/d\theta_c = 0$, $d^2V_0/d^2\theta_c = 0$, and, after straightforward algebraic calculations, we obtain the relations $I_{in} = \pi^2 V_{\rm FT}/\alpha\beta(\pi/2-\theta_c)^3\sin(2\theta_c)\sin(\beta\cos^2\theta_c)$, and $(\theta_c - \pi/2)[2\csc 2\theta_c + \beta\sin 2\theta_c\cot(\beta\cos^2\theta_c)] = 3$. The first expression gives the critical value of $I_{in}$ for which $V_0$ becomes multivalued. The second expression is an algebraic equation that depends only on the parameter $\beta$ and determines all the points of nascent bistability. Notice that only half of them have physical significance because the other half correspond to negative values of the intensity. By taking into account the constraint that the intensity must be positive and considering that the cotangent function is $\pi$ periodic, we have that the actual number of points of nascent bistability is equal to the next smallest integer of $\beta/2\pi$. For the values considered in our experiment, $\beta$ is about 54, then one expects to find eight points of nascent bistability in the entire $(V_0, I_{in})$ parameter space, a prediction that is confirmed by the experiment [10].

The dynamics around a nascent bistability point can be described by a scalar field $u(x,t)$ governed by a cubic nonlinearity. Hence, close to this point, $I_{in} \equiv I_{in}^c$, $V_0 \equiv V_0^c$, and we can consider

$$\theta(x,t) \approx \theta_c + u(x,t)/u_0, \quad (6)$$

where $u_0^2 \equiv 2\beta\cos 2\theta_c\cot(\beta\cos^2\theta_c) + (4+\beta^2\sin 2\theta_c)/3 - 2/(\pi/2-\theta_c)^2$ is a normalization constant.

Considering the above ansatz in Eq. (5) with a zero free propagation length $L = 0$, and developing in a Taylor series by keeping the cubic terms, after straightforward algebraic calculations, we can reduce the full LCLV model to a simple bistable model,

$$\tau\partial_t u = \eta + \mu u - u^3 + l^2\partial_{xx}u, \quad (7)$$

where $\eta \equiv \alpha[1-\cos(\beta\cos^2\theta_c)](\pi/2-\theta_c)^3[I_{in} - I_c + \alpha[1-\cos(\beta\cos^2\theta_c)(V_0 - V_c)]/2]/\pi^2 V_{\rm FT}$, and $\mu \equiv 12\Gamma\{(\pi/2-\theta_c)^2(V_0 - V_c) + [\pi^2 V_{\rm FT}/12 - (\pi/2-\theta_c)^2](I_{in} - I_c)/I_c\}/\pi^2 V_{\rm FT}$.

For a small free propagation length ($L \sim \epsilon \ll 1$), the light intensity $I_w$ reached in the photoconductor can be approximated by a local model characterized by

$$\begin{aligned} I_w(\theta,L) \approx I_{in}\{&1+\cos(\beta\cos^2\theta) \\ &+ L[1+\cos(\beta\cos^2\theta)\partial_{xx}\sin(\beta\cos^2\theta)]/k \\ &- L\sin(\beta\cos^2\theta)\partial_{xx}\cos(\beta\cos^2\theta)/k\}/2. \end{aligned}$$

Introducing this expression in Eq. (5), using ansatz (6), developing in a Taylor series by keeping the cubic terms in $u$, considering that the order parameter is a slow variable in space ($\partial_{xx}u \ll \partial_x u \ll 1$), renormalizing space, and after

straightforward calculations, we obtain Eq. (1), with

$$b = c \equiv -\frac{\pi\alpha\beta\cos(2\theta_c)I_c\left(\frac{V_{\rm FT}}{2V_c+\alpha I_c[1+\cos(\beta\cos^2\theta_c)]}\right)^{3/2}}{\sqrt{2}lu_0V_{\rm FT}}.$$

Hence, close to nascent bistability, model Eq. (5) can be approximated by a simple nonvariational model Eq. (1), which describes the complex dynamics observed around this critical point.

Numerical simulations of model (5) in the region of bistability for a small free propagation length show that the system exhibits front solutions. The front speed is affected when the free propagation length is changed. Therefore, these fronts present a propagation mechanism of a nonvariational nature.

*Experimental nonvariational front propagation.* Using the SLM, we have conducted quasi-one-dimensional experiments in a LCLV with optical feedback. As voltage $V_0$ is varied as a control parameter, we identify the bistable region, where two different molecular orientation states coexist. In this bistability region, the SLM is not only used to create a one-dimensional channel, but also to create localized perturbations, which allow us to observe the emergence of fronts between two different molecular orientations. Hence, the light observed in the near field has different intensities, which are associated with the molecular orientations. Figure 4(b) shows a temporal sequence of snapshots of front propagation. By recording the interface evolution over the channel with a CCD camera, we have measured the front speed, which is plotted in Fig. 4(c) as a function of $V_0$ for different values of free propagation length $L$. For small $L$, experimental imperfections are relevant. We consider nonsmall $L$. Note that as the free propagation length increases, the front speed increases, which is consistent with the theoretical prediction. Therefore, the mechanism that generates the spread of these fronts is the energy difference and front core shape (nonvariational effect).

In summary, we have characterized a mechanism of nonvariational front propagation in one-dimensional scalar fields, where the process responsible for generating the spread of this front is the front shape and not the energy difference between equilibria. In higher dimensions we expect that the propagation is only corrected by curvature effects, e.g., the Gibbs-Thomson effect [3].

*Acknowledgments*. M.G.C. and M.W. acknowledge funding from the FONDECYT Projects No. 1150507 and No. 3140387. A.J.A.-S. acknowledges financial support from Becas Conicyt 2015, Contract No. 21151618.

[1] P. Glansdorff and I. Prigogine, *Thermodynamic Theory of Structures: Stability and Fluctuations* (Wiley, New York, 1971).

[2] G. Nicolis and I. Prigogine, *Self-Organization in Nonequilibrium Systems* (Wiley, New York, 1977).

[3] L. M. Pismen, *Patterns and Interfaces in Dissipative Dynamics* (Springer, Berlin, 2006).

[4] M. Cross and H. Greenside, *Pattern Formation and Dynamics in Nonequilibrium Systems* (Cambridge University Press, New York, 2009).

[5] J. S. Langer, Instabilities and pattern formation in crystal growth, Rev. Mod. Phys. **52**, 1 (1980).

[6] W. van Saarloos, Front propagation into unstable states, Phys. Rep. **386**, 29 (2003).

[7] Y. Pomeau, Front motion, metastability and subcritical bifurcations in hydrodynamics, Physica D **23**, 3 (1986).

[8] P. Coullet, J. Lega, B. Houchmanzadeh, and J. Lajzerowicz, Breaking Chirality in Nonequilibrium Systems, Phys. Rev. Lett. **65**, 1352 (1990).

[9] M. G. Clerc, S. Coulibaly, and D. Laroze, Nonvariational Ising-Bloch transition in parametrically driven systems, Int. J. Bifurcation Chaos Appl. Sci. Eng. **19**, 2717 (2009); D. Michaelis, U. Peschel, F. Lederer, D. V Skryabin, and W. J. Firth, Universal criterion and amplitude equation for a nonequilibrium Ising-Bloch transition, Phys. Rev. E **63**, 066602 (2001).

[10] M. G. Clerc, A. Petrossian, and S. Residori, Bouncing localized structures in a liquid-crystal light-valve experiment, Phys. Rev. E **71**, 015205 (2005).

[11] S. Residori, Patterns, fronts and structures in a liquid-crystal-light-valve with optical feedback, Phys. Rep. **416**, 201 (2005).

[12] M. G. Clerc, T. Nagaya, A. Petrossian, S. Residori, and C. S. Riera, First-order Fréedericksz transition and front propagation in a liquid crystal light valve with feedback, Eur. Phys. J. D **28**, 435 (2004).

[13] F. Haudin, R. G. Elias, R. G. Rojas, U. Bortolozzo, M. G. Clerc, and S. Residori, Driven Front Propagation in 1D Spatially Periodic Media, Phys. Rev. Lett. **103**, 128003 (2009); Front dynamics and pinning-depinning phenomenon in spatially periodic media, Phys. Rev. E **81**, 056203 (2010).

[14] P. G. de Gennes and J. Prost, *The Physics of Liquid Crystals* (Oxford University Press, New York, 1995).

[15] M. Tlidi, P. Mandel, and R. Lefever, Localized Structures and Localized Patterns in Optical Bistability, Phys. Rev. Lett. **73**, 640 (1994).